

Design of an asymmetrical rotor for easy assembly and repair of field windings in synchronous machines

Nan Yang¹, Wenping Cao¹, Zheng Liu¹, John Morrow²

¹School of Engineering & Applied Science, Aston University, Aston Express Way, Birmingham B4 7ET, UK

²School of Electronics, Electrical Engineering and Computer Science, Queen's University Belfast, University Rd, Belfast BT7 1NN, UK

E-mail: w.p.cao@aston.ac.uk

Published in *The Journal of Engineering*; Received on 30th March 2017; Accepted on 19th June 2017

Abstract: This study introduces a new asymmetrical rotor design for easy assembly and repair of field windings in synchronous machines. A new rotor geometry is adopted in order to simplify the manufacture and maintenance process of installing the rotor windings. The asymmetrical rotor design is simulated by the two-dimensional finite element analysis, and verified by experimental tests on a 27.5 kVA prototype machine. The proposed topology can drive down the maintenance and repair costs of the machine without impacting on the machine's electro-magnetic performance. This design will have significant economic implications for machine design and repair industry, especially for mass production markets such as wind turbines and engine-generators.

1 Introduction

Wound rotor synchronous generators are widely used in industry, including steam turbines, diesel-generator sets (gen-sets) and wind turbines [1–3]. For steam turbines and diesel-generator sets, their synchronous machines are operated at a fixed speed. In wind turbines, variable-speed operation in synchronous machines is also applicable. In this case, gearboxes are required to convert the slow wind speed to the machine's synchronous speed whereas power converters are used to control the frequency and voltage for grid connection.

In wound-rotor synchronous machines, both stator and rotor windings are required. The installation of the stator winding is relatively simple. Pre-manufactured coils can be inserted into the stator slots one by one to form a three-phase distributed winding, as shown in Fig. 1. On the contrary, the rotor winding installation is laborious. In general, the rotor coils are wrapped around the rotor poles to form a DC excitation field. This can also be done by a winding machine, as shown in Fig. 2. The coils are wound around the pole shoes which are then mounted on top of the pole bodies. As the size of the rotor increases, the winding machine needs to be very large. Therefore, this installation becomes more challenging, costly and also affects the physical integrity of the rotor.

In addition, synchronous machines are prone to winding failures, which account for half of the total machine failures in the field [4]. When these machines break down, a decision should be made either to replace them or to repair them, usually based on an economic analysis. If a rewinding becomes necessary, the rotor winding will be removed and replaced by a new one. During the process, the rotor core and the machine efficiency can be affected [5]. If the rotor coils can be pre-produced and inserted into the rotor (similar to the stator winding), the winding machine can be made smaller and the manufacture costs be reduced significantly.

2 Literature review

This work addresses the manufacturing issue associated with the rotor field winding by modifying the rotor structure to allow for easy assembly of the rotor coils.

Traditional rotor design concentrates on changing the rotor geometry to establish the tradeoff between competing optimisation objects (such as volume to efficiency, mass to efficiency) [6]. The rotor designs are then modified and analysed by the finite element

analysis (FEA). A typical four pole synchronous machine is presented in Fig. 3. Their flux distributions and electro-magnetic performance can be obtained and compared.

Another interesting aspect of the rotor design is the use of magnets and flux barriers in the rotor. Two examples are shown in Fig. 4 for illustration.

These designs guide the flux to flow in chosen directions, as to enhance the air-gap flux density. This technology can be applied to variable types of machines such as synchronous reluctance machines [7–9], wound-rotor synchronous machines [10], and stator wound-field synchronous machines [11]. However, adding the flux barriers and magnets gives rise to the complexity and manufacture cost of the rotor. Therefore, this technology is not widely applied in industry.

Alternatively, claw-pole alternators can provide a simple winding installation solution [12]. As shown in Fig. 5, the field coils can be clicked into its position between the two rotor poles. However, this topology is quite complex electro-magnetically and the rotor is asymmetrical in the axial direction, a three-dimensional (3D) FEA tool must be used in order to determine its saturation level and leakage flux. This type of machine has quite high design and manufacture costs.

As far as the rotor pole geometry is concerned, asymmetrical rotors were reported in the literature [12–14]. These rotor designs are characterised with unequal pole numbers of the stator and rotor [15] or unbalanced rotor slot geometry [16].

Two asymmetrical rotor geometries are shown in Fig. 6. Both designs use the asymmetrical rotor geometry for reluctance machines which are not accepted by industry. This paper adopts an asymmetrical rotor design for the purpose of simplifying the assembly process of the rotor winding in the case of synchronous machines.

3 Proposed machine topology

Based on the existing rotor designs, a new rotor is developed in a way that the rotor coils can be installed to the pole directly. A 3D diagram of the proposed rotor is illustrated in Fig. 7. In the proposed topology, the field coils are pre-manufactured with insulation and covering. These coils are then installed onto the rotor pole from the tooth side and are fixed in the position between the rotor pole and rotor teeth, as illustrated in Fig. 8. Then, the coils can slide through the edge of the rotor onto the rotor pole. A non-magnetic



Fig. 1 Arrangement of the stator winding (distributed)

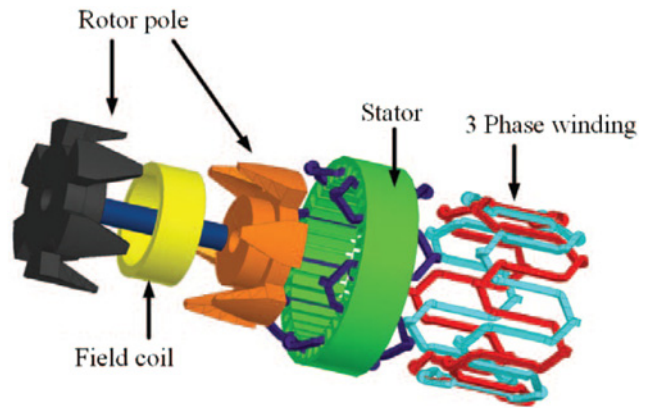


Fig. 5 Exploded view of the claw-pole machine [12]

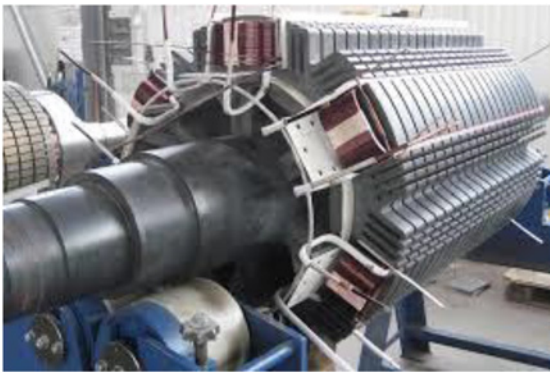


Fig. 2 Arrangement of the rotor winding (concentric)

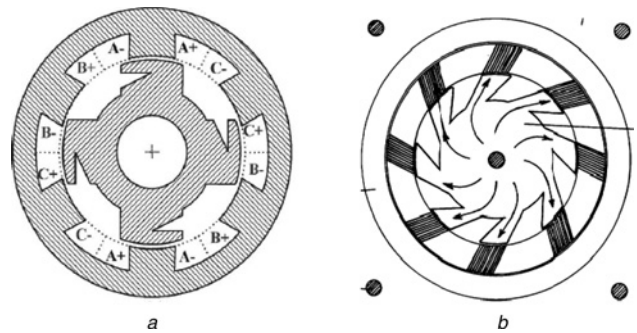


Fig. 6 Existing asymmetrical rotor designs
a Design 1 [13]
b Design 2 [17]

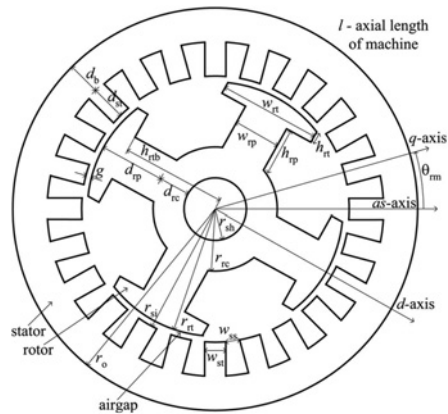


Fig. 3 Topology of traditional salient rotor for synchronous machines [6]

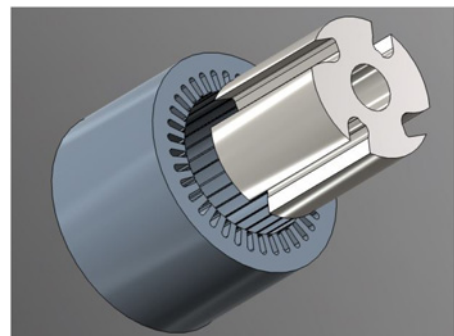


Fig. 7 3D diagram of the proposed machine

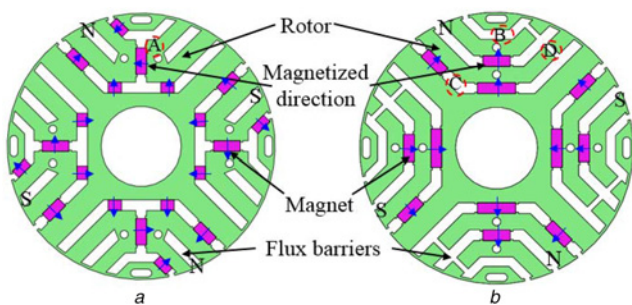


Fig. 4 Rotor designs with magnet-based flux barriers [7]
a Design 1
b Design 2



Fig. 8 Installation of the rotor coils

shield is installed in the position to fix the coils and to offset the centrifugal force.

In this machine, the segmentation of rotor poles is no longer necessary for rotor winding installation, making it easy to insert and remove the field coils. It maintains the integrity of the rotor and reduces the magnetic reluctance along the rotor path.

Because of the asymmetrical rotor shape, the machine's mechanical balance is affected. However, this is not a big problem in small and medium synchronous generators since they operate in relatively low speed and reasonably stable environments. The excitation winding are set to be wider than the rotor pole arm but the difference is small (<5% of the width of the winding). The empty space allows for more insulation and bonding materials to be applied so as to improve thermal transfer within the rotor. Clearly, the machine is designed to operate unidirectional, which is not an issue for applications such as steam turbines, gen-sets and wind turbines, which are the target of this work.

4 Finite element machine modelling

In order to evaluate the effectiveness of the proposed design, two 4-pole synchronous generators are modelled by the 2D finite element software MagNet. The two uses the same stator but two different rotors (one symmetrical and the other asymmetrical). The machine's stator is from a standard 27.5 kVA alternator while its salient rotor is used as a bench-mark against the new design.

4.1 No-load operation

A 2D transient analysis (with motion) of the proposed synchronous generator with DC excitation is first studied. The air-gap flux density, spatial harmonics, induced EMF at no-load conditions are obtained and shown in Figs. 9–13.

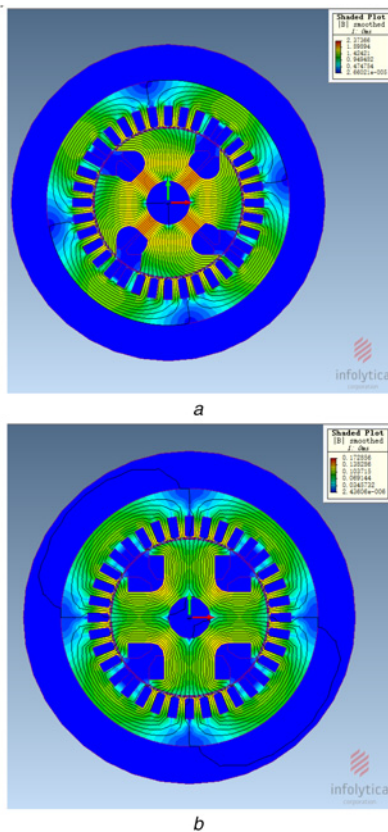


Fig. 9 Flux distribution of the machines at no-load
a Asymmetrical rotor
b Symmetrical rotor

As can be seen from Fig. 9, the direction of the flux in the asymmetrical rotor has been shifted towards one side. The absence of the rotor teeth on one side reduces the flux path, creating an unbalanced air-gap flux distribution. This introduces an angle between the rotor and stator fields. In this case, the magnetic flux is concentrated on the teeth side of the rotor, making the area easy to saturate. This feature is found on the induced EMF waveforms as well as its saturation level, as shown in Figs. 10–13.

Overall, the induced EMF, phase current and flux linkage between the two machines are similar. However, due to the asymmetrical pole geometry, the air-gap flux density of the new design is higher in the salient pole portion than the concave portion. This asymmetrical effect distorts the shape of the air-gap flux density along the rotor pole. The third harmonic of its air-gap flux density is increased while other high-order harmonics are reduced when compared to the symmetrical machine.

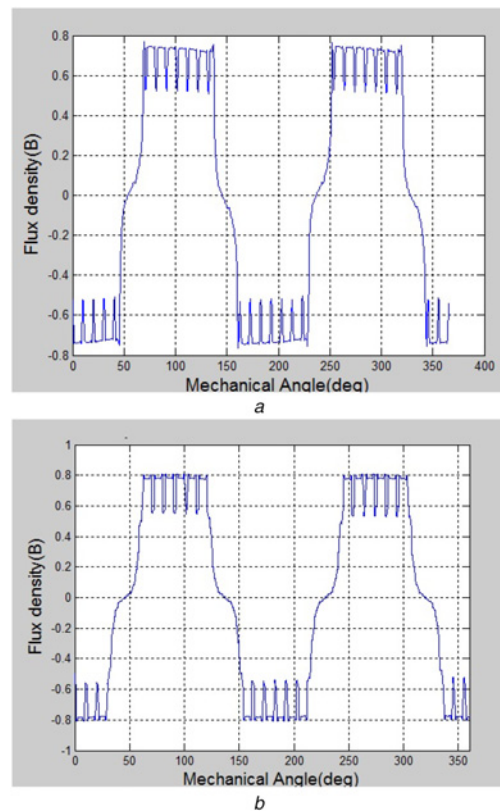


Fig. 10 No-load air-gap flux density
a Asymmetrical
b Symmetrical

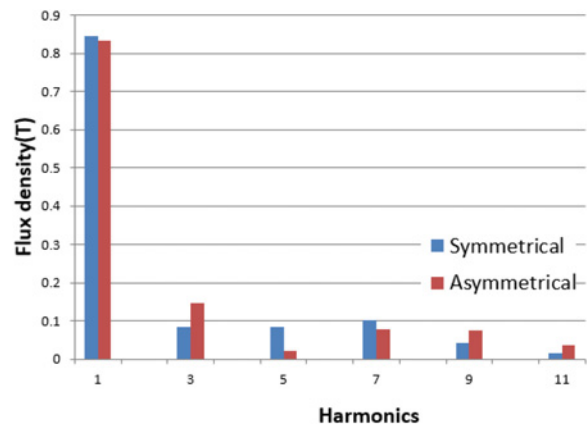


Fig. 11 FFT analysis of the no-load air-gap flux density

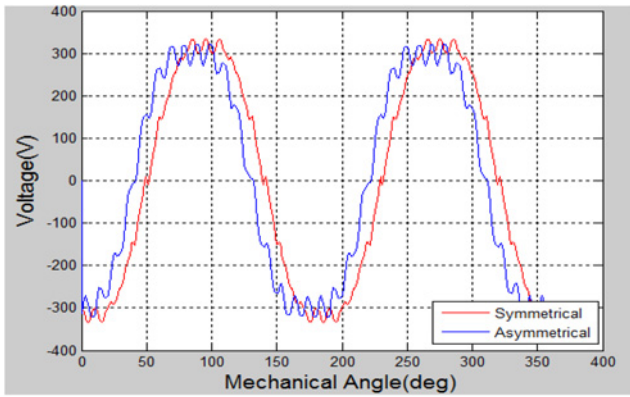


Fig. 12 No-load EMF voltages

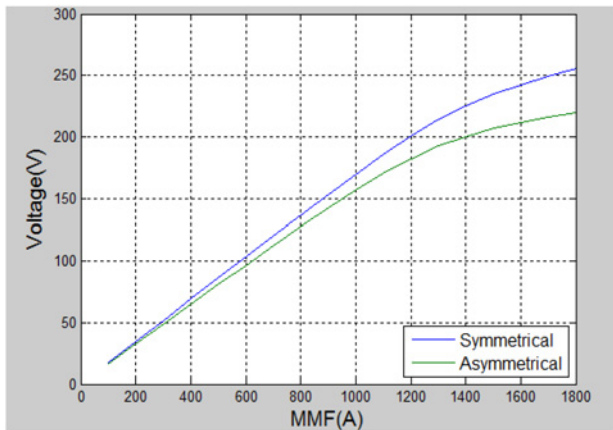


Fig. 13 No-load characteristics

Table 1 FFT analysis of the no-load EMF

Harmonics	Symmetrical rotor, Vrms	Asymmetrical rotor, Vrms
1	245.47	239.26
3	17.11	26.56
5	3.28	0.822
7	1.95	1.438
9	0.043	0.0234
11	0.162	0.772
THD, %	7.14	11.13

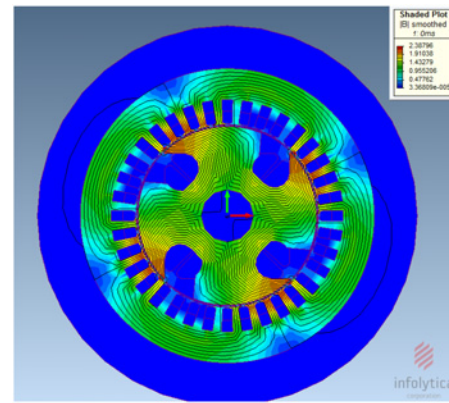
In addition to the air-gap flux density, a fast Fourier transform (FFT) analysis of the induced EMF is also conducted, as presented in Table 1. The THD of the asymmetrical rotor is still higher than its symmetrical counterpart as it gives rise to the third harmonics remarkably. This should be carefully examined in the design process.

From Fig. 13, it is observed that the asymmetrical machine reaches saturation earlier than the symmetrical as the excitation MMF increases. This is caused by the flux shift where the flux tends to concentrate on the salient side of the rotor.

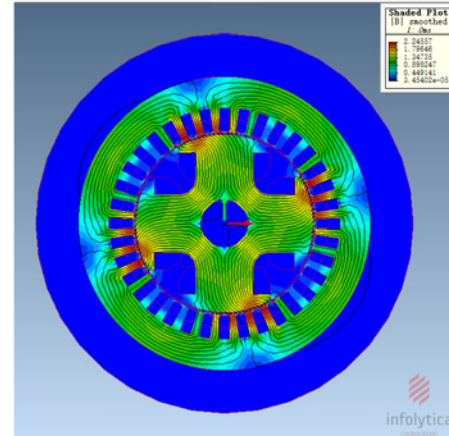
4.2 Full-load operation

The magnetic flux distribution of the two machines at full load operation is investigated when the field winding is excited with the rated DC current, and the stator windings are fed by the rated three-phase AC current (38 A peak).

Test results shown in Figs. 14–16 are the flux distribution, induced EMF, and the pull-out torque, respectively. Again,



a

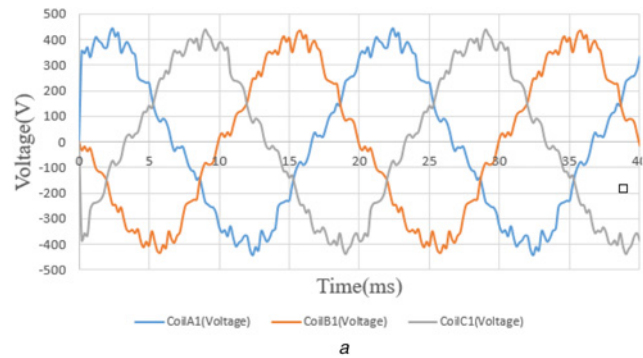


b

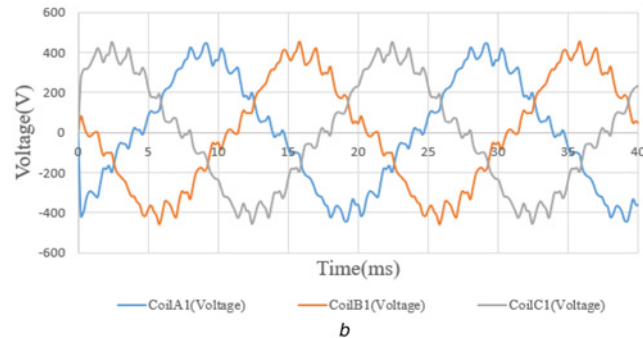
Fig. 14 Flux distribution of the machine at full-load

a Asymmetrical

b Symmetrical



a



b

Fig. 15 Induced phase voltages of the machines at full-load

a Asymmetrical

b Symmetrical

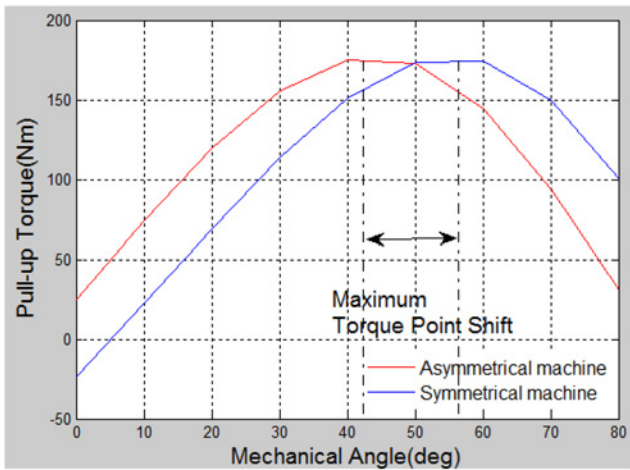


Fig. 16 Pull-out torques

the phase current and flux linkage in the two machines are very similar.

Due to the asymmetrical rotor geometry, the position of the machine for achieving maximum torque is also shifted. This angle can be explained by the difference of the stator and rotor field orientations. However, since most of the flux is concentrated on the teeth side of the rotor, the non-teeth side is not effectively utilised. Therefore, there is room for optimising the rotor pole geometry to improve the electro-magnetic efficiency.

4.3 Calculation of L_d and L_q

The measurement of the direct-axis reactance and quadrant-axis reactance is carried by a low-slip test following the standard method [10]. The rotor is driven by a prime mover to rotate at 1483.3 rpm (0.01 slip) while the field winding is open-circuited. The stator is fed with a 50 Hz, 4 A AC current. The relative position of the stator and rotor magnetic fields is changing to reflect the different air-gap distance, and the test results are presented in Fig. 17.

The maximum and minimum flux-linkages for the asymmetrical rotor are 0.094 and 0.068 Wb, respectively. The direct-axis and quadrant-axis reactances are

$$L_d = 0.094/2 = 0.047 \text{ H}, \quad X_d = \omega L_d = 7.3 \Omega \quad (1)$$

$$L_q = 0.068/2 = 0.034 \text{ H}, \quad X_q = \omega L_q = 5.3 \Omega \quad (2)$$

The maximum and minimum flux-linkages for the symmetrical rotor are 0.093 and 0.061 Wb, respectively,

$$L_d = 0.092/2 = 0.046 \text{ H}, \quad X_d = \omega L_d = 7.15 \Omega \quad (3)$$

$$L_q = 0.061/2 = 0.031 \text{ H}, \quad X_q = \omega L_q = 4.82 \Omega \quad (4)$$

Due to the transformation of the rotor geometry, saliency of the rotor has been changed. This saliency change has its impact on the torque output of the alternator. Per the equations in [10], the output torque at any speed can be derived as

$$T = X_{ad} I_f I_s \cos \gamma - \frac{1}{2} (X_d - X_q) I_s^2 \sin 2\gamma \quad (5)$$

where X_d , X_{ad} , per unit direct-axis synchronous and magnetising reactance at one per unit speed; and X_q , per unit quadrature-axis reactance at one per unit speed.

With V_s defined as the stator voltage and I_s as the phase current, the first component of the equation can be considered as the stator-rotor field interaction. The second part is the reluctance torque caused by

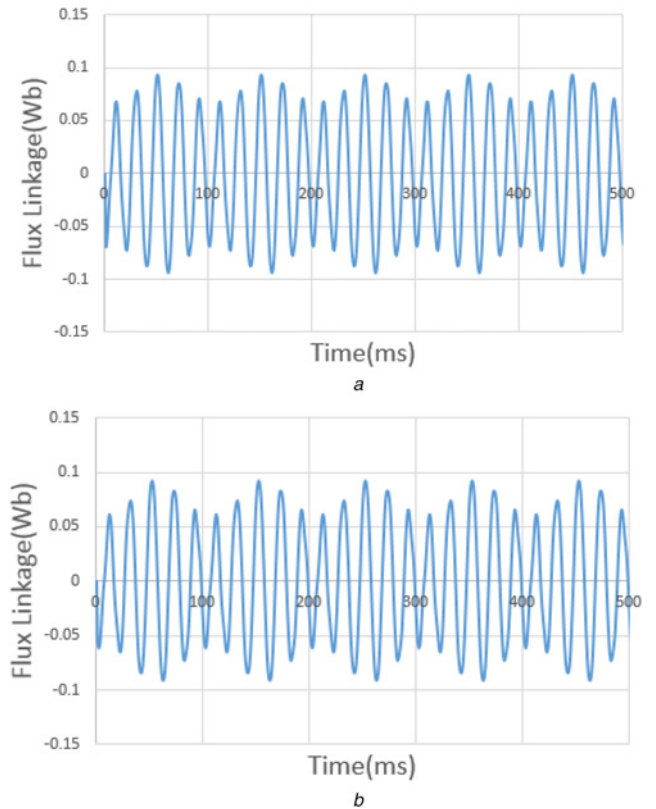


Fig. 17 Simulated low-slip test results

a Asymmetrical
b Symmetrical

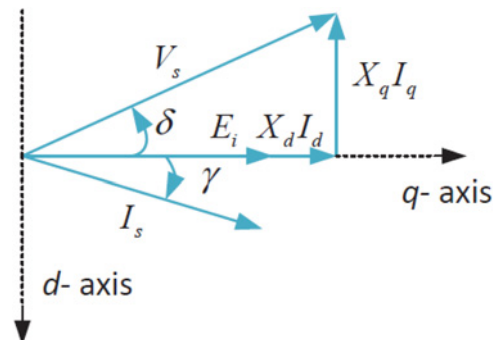


Fig. 18 Phasor diagram

the saliency of the rotor. A phasor diagram of the salient pole wound rotor synchronous machine is shown in Fig. 18.

Obviously, given by the measurement of d - q reactance, the rotor geometry change should have its impact on the torque production. Therefore, it is possible to modify the saliency of the rotor by modifying the geometry of the rotor instead of introducing extra component into the rotor.

4.4 Power loss and efficiency

The core loss and copper losses are calculated using the Infolytica MagNet. The data are shown in Table 2.

From this table, the two designs have the same copper loss due to the same stator configuration and supply. The asymmetrical machine has a slightly lower torque and iron loss. With the same input power, the asymmetrical machine has a lower efficiency than the symmetrical machine. However, this reduction is very insignificant.

Table 2 Loss and efficiency of tow synchronous generators

Item	Asymmetrical rotor	Symmetrical rotor
copper loss, W	216	216
iron loss, W	384	397
torque, Nm	153.7	158.6
speed, rpm	1500	1500
efficiency, %	97.4	97.5

5 Experimental tests and result analysis

After a round of optimising the rotor design and analysing the machine performance, the rotor design is finalised and the rotors are prototyped, as shown in Fig. 19.

Stator of the machine is a duplicate of a standard Cummins BCI-184F machine. Two rotors are manufactured for compare. Details of the machine are given in Table 3.

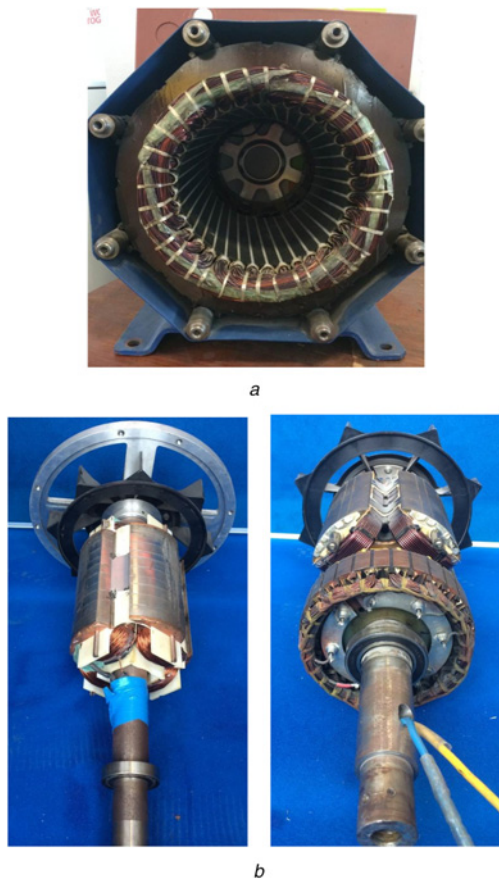


Fig. 19 Photos of the prototyped synchronous machine
a Stator
b Asymmetrical and symmetrical rotors

Table 3 Specifications of two generators

rated power, kVA	27.5	rated speed, rpm	1500
rated voltage, V	380	rated frequency, Hz	50
rated power factor	0.8	stack length, mm	200
stator slot number	36	pole numbers	4
stator OD, mm	310	stator ID, mm	192
rotor OD, mm	188	stator winding arrangement	Double-layer star

For stator windings, they are double-layer star connected windings with 144 mm² for each layer. For rotor windings, 76 turns of copper coil (2.3 mm radius each) are used on symmetrical rotor coils. However, due to the manufacture requirement, asymmetrical rotor adopts hand-wounded 1.5 mm copper wires with 200 turns. This will affect the rated excitation current so the MMFs are used to describe the excitation in the following experiments.

A series of experimental tests have been conducted on the proposed machine with the two different rotors.

5.1 Constant speed-variable excitation test

A constant speed-variable excitation test is conducted by coupling the test machine with a DC drive motor. The DC motor is used as prime-mover for keeping the speed of the rotor at synchronous speed (1500 rpm). The stator is open-circuited and connected to a three-phase power analyser to record the instantaneous quantities. The excitation is fed from a three-phase AC supply through a rectifier. The excitation current is measured by an ammeter at the output terminal of the rectifier.

When carrying the no-load test, the excitation is changed in step from high to low voltage using approximately even distributed points, starting from the rated value down to zero following the IEEE standard procedure. The armature voltage (in RMS) at the terminal versus the excitation current (in per unit) at rated speed is plotted in Fig. 20.

It is clear that the performance of the two machines is similar with the asymmetrical machine more likely to enter saturation earlier than the symmetrical one.

The reason is as stated in the previous chapter. The concentration of the flux on the teeth-side of the rotor makes the asymmetrical rotor easier to saturate. The comparison between FEA simulation and experiment results is also included in this figure to confirm the accuracy of the FEA simulation.

5.2 Constant excitation-variable speed test

In this test, the excitation is fixed while the DC motor drives the test machine to rotate at variable speeds. The armature phase voltage is plotted against speed in Figs. 21 and 22. Again, the two machines perform almost identically.

5.3 Sustained three-phase short-circuit test

The sustained three-phase short-circuit test is carried out by keeping the rotor speed at 1500 rpm while three-phase windings are short-circuited at the stator terminals. The short-circuit current is recorded. The excitation is adjusted in steps from high to low current using approximately even distributed points, starting from

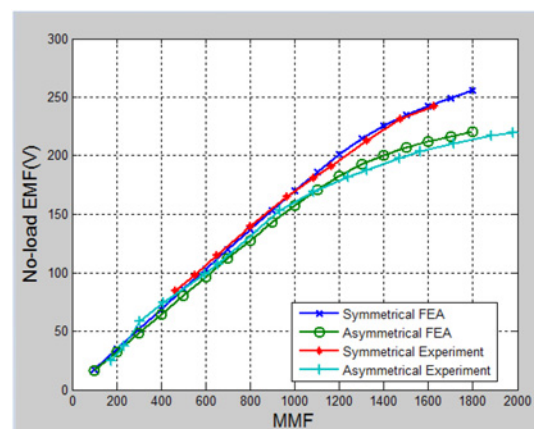


Fig. 20 Comparison of the constant speed-variable excitation test between the two machines

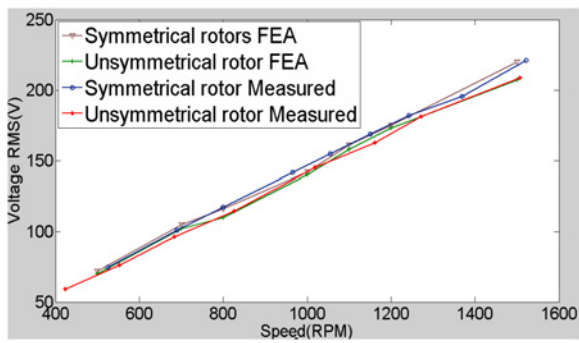


Fig. 21 FEA and measured results of the output voltage

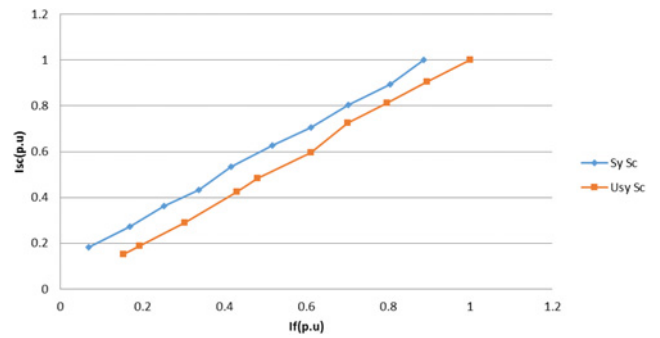


Fig. 23 Comparison of the two machines in sustained three-phase short-circuit test

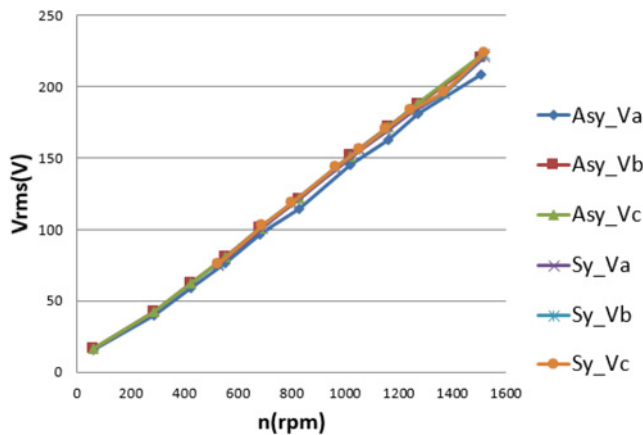


Fig. 22 Comparison of constant excitation-variable speed test between the two machines

the rated excitation current. The armature currents are measured at the terminals. The armature current versus the excitation current at rated speed is shown in Fig. 23.

For a given excitation current, the short-circuit current in the asymmetrical machine is lower than the symmetrical one. This should be carefully examined in the fault analysis since the short-circuit current is smaller.

5.4 Inductive load test

Inductive loads are the most common type of loads connected to the power system. Therefore, the machine's response to such load changes is of critical importance in terms of the system stability. This load test is designed to compare the performance of the two designs under the same conditions. In the test, the stator terminals are connected to a power analyser in parallel with an inductive load bank. The phase voltage and current are measured by the power analyser and the excitation is measured by an ammeter at the output terminal of the rectifier.

The excitation current is initially adjusted to achieve a given armature voltage (i.e. rated EMF). Then, the inductive load is gradually increased from 0 to 5 kW in steps. The voltage and current are recorded, and presented in Fig. 24. The test results show that the EMF voltage of the machine with the asymmetrical rotor is less sensitive to the load variations. As a result, the proposed design can improve the system stability under load variations.

5.5 Resistive load test

The resistive load test has the same setting as the inductive load test. The voltage and current are recorded as well as the load. The test results are presented in Fig. 25.

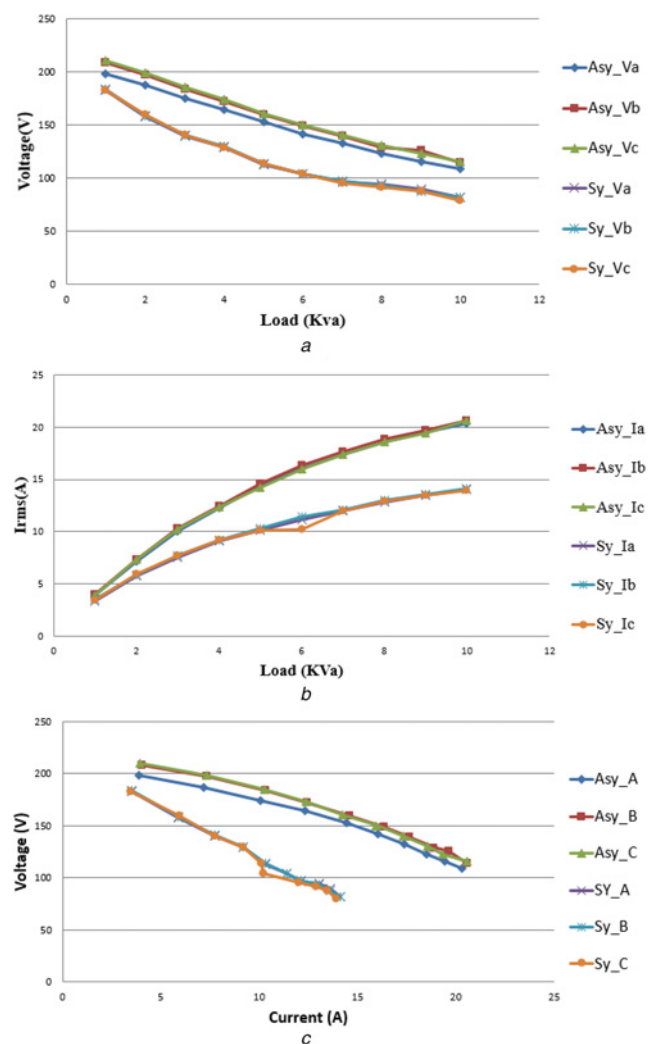


Fig. 24 Comparison of the two machines at varying inductive loads

Test results show the same trend as the inductive load test. The asymmetrical rotor performed better in both cases. This confirms the excellent performance of the proposed machine under different load conditions.

Through simulation and experimental tests, the effectiveness of the asymmetrical rotor design is verified. In addition to the modified rotor geometry for easy assembly, the designed rotor also shows potential in saliency-enhancement. However, it is also noticed that this design suffers from high saturation level as well as lower power factor. Therefore, further optimisation should be considered in further studies.

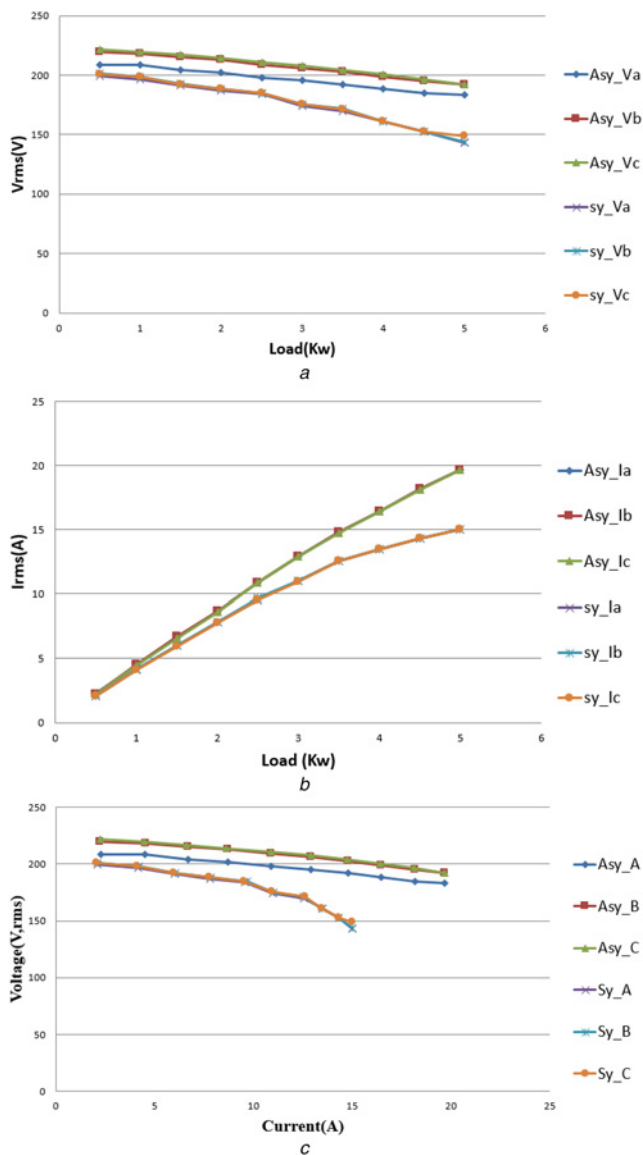


Fig. 25 Comparison of the two machines at different resistive loads

6 Conclusion

This paper has presented a new rotor design of synchronous generators targeted for diesel-engine-generating sets. The rotor pole is asymmetrical, effectively shifting the magnetic field to change the saliency of the rotor. As a result, the power output is influenced as well as its power factor range.

By adopting an asymmetrical rotor geometry, field windings can be easily installed on the rotor, thus simplifying machine assembly and repair procedures. Simulation results from 2D FEA and experimental results from testing a 27.5 kVA prototype machine have verified the new rotor design. Overall, the power profile can be improved, in addition to easy assembly of the field windings.

The developed technique can significantly reduce the maintenance and repair costs of synchronous generators, especially for those very large alternators and for mass production markets such as gen-sets and wind power generation. Machine designers, manufacturers and repairers can benefit from this design in terms of reduced capital and maintenance costs.

7 References

- [1] Daley J.M., Siciliano R.L.: 'Application of emergency and standby generation for distributed generation. I. Concepts and hypotheses', *IEEE Trans. Ind. Appl.*, 2003, **39**, (4), pp. 1214–1225
- [2] Hassan I., Weronick R., Bucci R., *ET AL.*: 'Evaluating the transient performance of standby diesel-generator units by simulation', *IEEE Trans. Energy Convers.*, 1992, **7**, (3), pp. 470–477
- [3] Martin J., Tindall C., Morrow D.J.: 'Synchronous machine parameter determination using the sudden short-circuit axis currents', *IEEE Trans. Energy Convers.*, 1999, **14**, (3), pp. 454–459
- [4] Stone G.C., Culbert I., Boulter E.A., *ET AL.*: 'Salient pole rotor winding failure mechanisms and repair', in 'Electrical Insulation for Rotating Machines: Design, Evaluation, Aging, Testing, and Repair' (Wiley-IEEE Press, Hoboken, NJ, USA, 2014), pp. 253–263
- [5] IEEE Std 1068-2015 (Revision of IEEE Std 1068-2009): 'IEEE Standard for the Repair and Rewinding of AC Electric Motors in the Petroleum, Chemical, and Process Industries', 2006
- [6] Smith T., Jones M.: 'Modeling of salient-pole wound-rotor synchronous machines for population-based design', *IEEE Trans. Energy Convers.*, 2011, **26**, (2), pp. 381–392
- [7] Zhao W., Chen D., Lipo T.A., *ET AL.*: 'Performance improvement of ferrite-assisted synchronous reluctance machines using asymmetrical rotor configurations', *IEEE Trans. Magn.*, 2015, **51**, (11), pp. 1–4
- [8] Vartanian R., Toliyat H.A.: 'Design and comparison of an optimized permanent magnet-assisted synchronous reluctance motor (PMA-SynRM) with an induction motor with identical NEMA Frame stators'. 2009 IEEE Electric Ship Technologies Symp., 2009, pp. 107–112
- [9] Prieto D., Dagusé B., Dessante P., *ET AL.*: 'Effect of magnets on average torque and power factor of synchronous reluctance motors'. 2002 IEEE XXth Int. Conf. Electrical Machines (ICEM), 2012
- [10] Liu W., Lipo T.A.: 'On saliency enhancement of salient pole wound field synchronous machines'. 2016 IEEE Energy Conversion Congress and Exposition (ECCE), 2016
- [11] Zhu Z., Zhou Y., Chen J., *ET AL.*: 'Investigation of nonoverlapping stator wound-field synchronous machines', *IEEE Trans. Energy Convers.*, 2015, **30**, (4), pp. 1420–1427
- [12] Liu H.-C., Jeong G., Ham S.-h., *ET AL.*: 'Optimal rotor structure design of claw-pole alternator for performance improving using static 3D FEM coupled-circuit model'. 2016 IEEE Conf. Electromagnetic Field Computation (CEFC), 2016
- [13] Li G., Ojeda J., Hlioui S., *ET AL.*: 'Modification in rotor pole geometry of mutually coupled switched reluctance machine for torque ripple mitigating', *IEEE Trans. Magn.*, 2012, **48**, (6), pp. 2025–2034
- [14] Harianto C.A., Sudhoff S.D.: 'A rotationally asymmetric reluctance machine with improved torque density', *IEEE Trans. Energy Convers.*, 2013, **28**, (1), pp. 62–75
- [15] Zhao W., Lipo T.A., Kwon B.-I.: 'Optimal design of a novel asymmetrical rotor structure to obtain torque and efficiency improvement in surface inset PM motors', *IEEE Trans. Magn.*, 2015, **51**, (3), pp. 1–4
- [16] Chitroju R., Sadarangani C.: 'Phase shift method for radial magnetic force analysis in induction motors with non-skewed asymmetrical rotor slots'. IEEE Int. Electric Machines and Drives Conf., 2009 IEMDC'09, 2009
- [17] Aspden H.: 'Magnetic reluctance motor'. UK Patent GB2303255A, 1997